AIAA JOURNAL
Vol. 39, No. 7, July 2001

Characterization and Analysis of Magnetorheological Damper Behavior Under Sinusoidal Loading

Rebecca A. Snyder,* Gopalakrishna M. Kamath,† and Norman M. Wereley‡
University of Maryland, College Park, Maryland 20742

The hysteresis behavior of a linear stroke magnetorheological damper is characterized for several magnetic fields and sinusoidal excitations over a nominal operational frequency range of 1.0–3.0 Hz. The behavior of the damper is inadequately modeled using the equivalent viscous damping and the complex modulus. Therefore, four different nonlinear modeling perspectives are discussed for purposes of system identification procedures, including the 1) nonlinear Bingham plastic model, 2) nonlinear biviscous model, 3) nonlinear hysteretic biviscous model, and 4) nonlinear viscoelastic plastic model. The first three nonlinear models are piecewise continuous in velocity. The fourth model is piecewise smooth in velocity. The parameters for each model are identified from an identification set of experimental data; these parameters are then used to reconstruct the force vs displacement and the force vs velocity hysteresis cycles for the respective model. Model performance is evaluated by calculating equivalent viscous damping and force time history errors between the model fit and the experimental data. In addition to the identification study, a validation study was done. Model parameters were calculated for offset values of current and frequency. These intermediate parameters were used to calculate hysteresis cycles, which were compared with a second set of experimental data, a validation data set. Identification and validation study results including damping levels and force time history errors.

Nomenclature

$a(t)$ = acceleration input to damper shaft
C_{eq} = equivalent (linearized) viscous damping
C_{po} = postyield viscous damping [nonlinear hysteretic biviscous (NHBV)]
C_{pr} = preyield viscous damping (NHBV)
C_{ve} = preyield viscoelastic damping [nonlinear viscoelastic plastic (NVEP)]
C_{vi} = postyield viscous damping (NVEP)
E = energy dissipated by damper
F_c = yield force constant (NVEP)
F_y = yield force (NHBV)
$f(t)$ = force measurement
I = applied current
K_{ve} = preyield viscoelastic stiffness (NVEP)
K^* = damper complex stiffness
K' = damper in-phase or storage stiffness
K'' = damper quadrature or loss stiffness
S_c = yield force shape function
S_{ve} = preyield viscoelastic shape function
S_{vi} = postyield viscous shape function
$v(t)$ = velocity input to damper shaft
v_y = yield velocity
v_0 = zero force velocity intercept
v_1 = compressive yield velocity
v_2 = tensile yield velocity
X_0 = sinusoidal displacement amplitude
$x(t)$ = displacement input to damper shaft
ϵ_c = yield force shape function parameter (NVEP)
ϵ_y = yield shape function parameter (NVEP)
Ω = frequency of sinusoidal damper excitation

Presented as Paper 98-2040 at the AIAA/ASME/AHS Adaptive Structures Forum, Long Beach, CA, 20–23 April 1998; received 10 August 1998; revision received 18 March 1999; accepted for publication 25 September 2000.

*Graduate Research Assistant, Smart Structures Laboratory, Alfred Gessow Rotorcraft Center, Department of Aerospace Engineering; rebsny@glue.umd.edu. Member AIAA.

†Research Scientist, Smart Structures Laboratory, Alfred Gessow Rotorcraft Center, Department of Aerospace Engineering; currently Scientist, National Aerospace Laboratories, Bangalore 560 017, India.

‡Associate Professor of Aerospace Engineering, Smart Structures Laboratory, Alfred Gessow Rotorcraft Center, Department of Aerospace Engineering; wereley@eng.umd.edu. Member AIAA.

I. Introduction

ELECTRORHEOLOGICAL (ER) and magnetorheological (MR) fluids belong to the class of smart materials that have the unique ability to change properties when electric or magnetic field is applied. When field is applied to an ER or MR fluid, this change is primarily manifested as a substantial increase in the dynamic yield stress of the fluid, while the viscosity remains relatively constant.[1] When compared to ER fluids, MR fluids have superior properties, including an order of magnitude higher yield stress, typically 50–100 kPa, and a much wider operational temperature range, typically −40 to 150°C. High payoff can result by applying these materials in dampers for aerospace systems such as the lag mode damper for stability augmentation of helicopter rotor systems,[2] dampers for landing gear to enhance crashworthiness,[3,4] and shock and vibration isolation mounts for avionics packages.

A critical element in the design of such systems is the evaluation of system dynamics via simulation, for which the nonlinear behavior of the semiactive ER/MR damper must be properly represented. The damper model also plays an important role in the choice of the control strategy for a given application. Some of the existing semiactive control strategies assume a linear damper model (a purely viscous element or a Kelvin chain) with field-dependent coefficients.[5,6]

There are several potential pitfalls in assuming a linear damper model for the MR damper. The major problem with the linear model is the inability to capture the nonlinear dynamic behavior, or nonelliptical force vs displacement hysteresis cycle, exhibited during sinusoidal excitations. Linear models can predict equivalent viscous energy dissipation but are unable to predict force response. Although the damping is modeled well, these linear models represent the force response of the MR damper as a dashpot with a constant value for damping. However, the MR damper operates in two distinct regions, low speed and high speed, each with its own distinct value of damping.

Other problems with using a linear model to describe nonlinear dampers are discussed by Kunz,[7] as applied to helicopter lag dampers. The behavior of a lag damper is dependent upon amplitude and frequency of motion. These factors cause nonlinearities in the damper behavior, which linear models such as the equivalent viscous damping and the complex modulus cannot capture. Another drawback to the equivalent viscous damping and the complex

modulus is that they are frequency dependent; therefore, these linear models can only be used to predict the steady-state response of a linear damper.[8] Presented in this paper is a comparative analysis of models that can be used to describe ER/MR damper behavior in this context for steady state sinusoidal excitation.

We present four mechanisms-based modeling perspectives with which to analyze the nonlinear damper behavior: 1) the Bingham plastic model,[9,10] 2) the nonlinear biviscous model,[11,12] 3) the nonlinear hysteretic biviscous model,[13] and 4) the nonlinear viscoelastic plastic model.[8,14,15] In these models force vs velocity damper behavior is extrapolated from analogous shear stress vs shear rate constitutive behavior of ER/MR fluids. The first three models are piecewise continuous in velocity. These models increase in complexity by adding progressively more parameters. The fourth model, the nonlinear viscoelastic plastic model, is piecewise smooth in velocity. The nonlinear hysteretic biviscous model can be used to motivate our nonlinear viscoelastic plastic model[8,14,15] and to improve the parameter optimization procedures used to identify its parameters. Other generalized hysteresis models have been proposed for MR dampers of this type, such as Bouc–Wen hysteresis model.[16,17] However, our objective is to improve understanding of force vs displacement and force vs velocity damper behavior by developing a mechanisms-based modeling perspective.

Along with characterizing the behavior of the MR damper based on experimental data, we will demonstrate the ability of the nonlinear hysteretic biviscous and the nonlinear[8,14,15] viscoelastic plastic models to capture both the force vs displacement and force vs velocity behavior of the damper over its entire operating range. Model parameters for each of the four models are identified using an experimental data set. These parameters were used to both reconstruct the hysteresis cycles, which are compared with the experimental data from the identification data set, and to interpolate values for the model parameters for different frequencies and applied currents. The identified model is then validated using a second validation data set. Interpolated model parameters are used to reconstruct the hysteresis cycle data in the validation set. Again, the error between predicted and measured damping and force time histories is calculated. This allows an assessment of the model performance for data not used in its identification.

A systematic procedure with which to analyze the hysteresis behavior caused by steady-state sinusoidal excitation of MR dampers. Because the rheological behavior of ER fluids is qualitatively similar to that of MR fluids,[18] these results can also be extended to ER dampers. We will evaluate the performance of these models by comparing model identification and predictions with experimental force vs displacement and force vs velocity hysteresis cycle data.

II. Damper Testing

The magnetorheological (MR) linear stroke damper used for this study is a commercially available truck seat damper manufactured by the Lord Corporation. This damper was chosen in order to present a case study that can easily be replicated. A schematic of the nominal MR damper is shown in Fig. 1a. The hydraulic cylinder of the damper is nominally 102 mm (4 in.) in length and 45 mm (1.75 in.) in diameter. As shown in Fig. 1a, the hydraulic cylinder houses the damper piston, in which is mounted a magnetic circuit. At the base and inside the hydraulic cylinder is a nitrogen accumulator that is used to pressurize the approximately 50 ml of MR fluid to above atmospheric pressure. This is a standard technique used to prevent cavitation on the low pressure side of the piston while it is in motion. The MR fluid flows through an annular orifice in the piston head, where it can be activated by a current applied to the magnetic circuit. Additional discussions of this damper are given by Dyke et al.[16] and Spencer et al.[17]

The MR damper was tested in order to determine steady-state characteristics for sinusoidal velocity inputs. Testing of the MR damper was done at varying frequencies and magnetic fields, thus creating two separate test matrices. The first data set was used to identify model parameters. The identification data were collected using applied currents in the range of 0–1.0 A in increments of 0.2 A, with a sinusoidal excitation of the damper shaft through a frequency range of 1.00–3.00 Hz in increments of 0.25 Hz. To create a magnetic field inside the damper, electric current is used to activate a magnetic circuit. Measurements of magnetic field applied to the damper are not available; hence, applied current is used to gauge magnetic field strength. The validation, or second, data set is used to validate the hysteresis cycles reconstructed from interpolated model parameters of the nonlinear hysteretic biviscous and the nonlinear viscoelastic plastic models. For this test matrix the damper was tested using current ranging from 0–0.9 A in increments of 0.2 A. The frequencies tested for the validation data set range from 1.125–2.875 Hz in increments of 0.25 Hz. The test conditions for the identification and validation experimental matrices are shown in Tables 1 and 2, respectively.

Table 1 Tested 54 unique operating conditions to create an identification data set

Applied current	Sinusoidal frequency Ω, Hz								
I, A	1.00	1.25	1.50	1.75	2.00	2.25	2.50	2.75	3.00
0	×	×	×	×	×	×	×	×	×
0.2	×	×	×	×	×	×	×	×	×
0.4	×	×	×	×	×	×	×	×	×
0.6	×	×	×	×	×	×	×	×	×
0.8	×	×	×	×	×	×	×	×	×
1.0	×	×	×	×	×	×	×	×	×

Table 2 Tested 48 unique operating conditions to create a validation data set

Applied current	Sinusoidal frequency Ω, Hz							
I, A	1.125	1.375	1.625	1.875	2.125	2.375	2.625	2.875
0	×	×	×	×	×	×	×	×
0.1	×	×	×	×	×	×	×	×
0.3	×	×	×	×	×	×	×	×
0.5	×	×	×	×	×	×	×	×
0.7	×	×	×	×	×	×	×	×
0.9	×	×	×	×	×	×	×	×

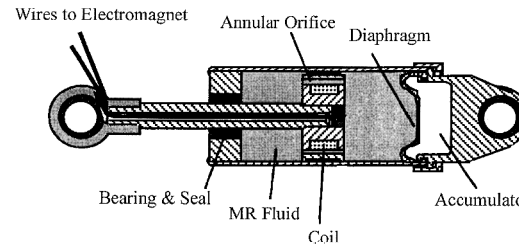

Fig. 1a Cross section of the Rheonetics SD-1000-2 MR damper. Courtesy of Lord Corporation.

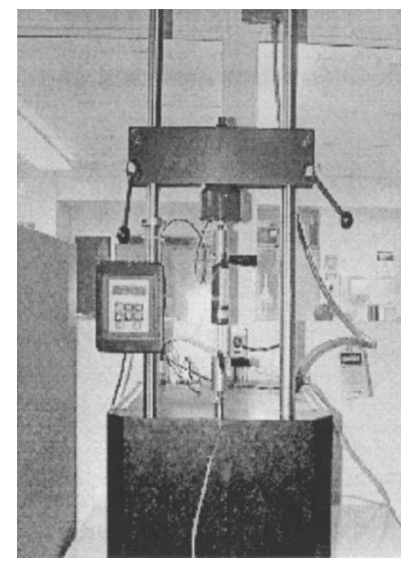

Fig. 1b Mechanical damper dynamometer used for damper testing.

MR damper testing was done using a 5-hp Roehrig Engineering mechanical damper dynamometer, as shown in Fig. 1b. A sinusoidal shaft displacement of 25.4-mm (1-in.) amplitude, measured using a linear variable differential transformer, was used to excite the dampers and the resulting force was measured using a load cell. The resulting force vs displacement and force vs velocity hysteresis cycles were measured for every test condition in each test matrix. Applied current, and hence magnetic field, was controlled using a power supply, which provided current to the electromagnet inside the damper.

III. Filtering of Data

During each test, nominally one cycle of force vs displacement data was measured, and the force vs velocity hysteresis cycle was calculated.

Calculating the velocity and acceleration signals using a finite difference method tended to accentuate noise, especially in the acceleration signal. Instead, the velocity and acceleration were calculated by differentiating a Fourier-series expansion. A periodic Fourier series was used to minimize the effects of this noise in the input displacement signal and the subsequent differentiations to obtain the input velocity and acceleration signals.[19]

The force signal was not filtered because the damper response was nonlinear and it could not be determined a priori exactly which harmonics contributed to the damper response and/or noise. Therefore, we conservatively used the measured (unfiltered) force data in both the model parameter identification and prediction studies.

IV. Experimental Results

Typical filtered hysteresis data is shown in Fig. 2. The force vs displacement [$f(t)$ vs $x(t)$] and the force vs velocity [$f(t)$ vs $v(t)$] hysteresis cycles show applied currents of 0.2, 0.4, 0.6, and 1.0 A at a frequency of $\Omega = 2.00$ Hz.

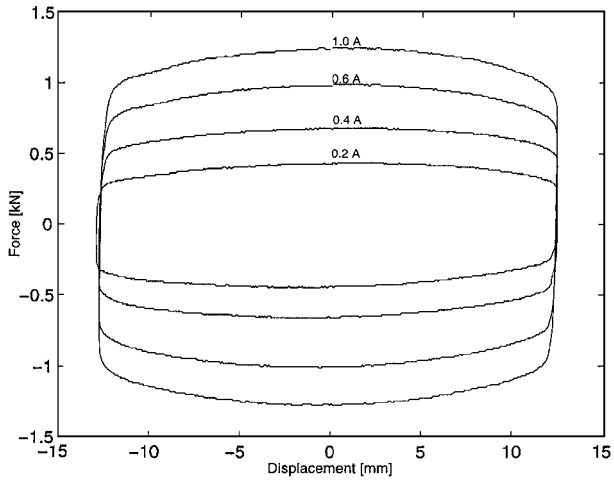

a) Force vs displacement

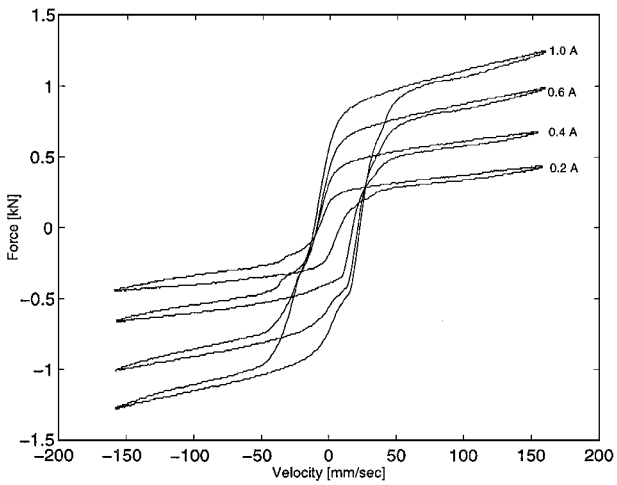

b) Force vs velocity

Fig. 2 Hysteresis cycles for the MR damper for sinusoidal excitation at 2 Hz.

As shown in Fig. 2a, as the applied current to the electromagnet is increased the magnetic field increases, and hence the amount of damping also increases, which is represented by the increasing area enclosed by the force vs displacement hysteresis cycle. The Bingham plastic-like behavior[20,21] of the MR damper can be seen in the force vs velocity hysteresis cycles as shown in Fig. 2b. Consider the high-velocity asymptote of an individual force vs velocity hysteresis cycle. If this asymptote is projected back to the force axis, this intercept gives the value of the yield force F_y. It is easily seen that this yield force increases as the applied current (magnetic field) increases. When the damper restoring force is less than this yield force, the damper is said to be operating in the preyield region. When the restoring force is greater than the yield force, the damper is said to be operating in the postyield region. The yield transition occurs as the damper restoring force transitions through the yield force value.

V. Linear Damper Models

A. Equivalent Viscous Damping

Equivalent viscous damping is a standard linearization technique that could be applied to a nonlinear damper such as this MR damper. Here, the damper restoring force $f(t)$ is proportional to damper shaft velocity $v(t)$ as

$$f(t) = C_{\text{eq}} v(t) \tag{1}$$

The equivalent viscous damping C_{eq} is computed by equating the energy dissipated over a cycle E at frequency Ω using

$$E = \oint F(t)\,\mathrm{d}x = \int_0^{2\pi/\Omega} F(t)v(t)\,\mathrm{d}t \tag{2}$$

and equating the dissipated energy of the nonlinear device to that of an equivalent viscous damper:

$$C_{\text{eq}} = E \big/ \pi \Omega X_0^2 \tag{3}$$

The energy dissipated over one cycle is computed using the trapezoidal rule. The equivalent viscous damping is calculated using Eq. (3) for each test case. The results from the identification set are shown in Fig. 3. As a result of this characterization procedure, the damper is linearized to be an ideal dashpot at every operating condition so that C_{eq} is a function of both the input current I and the displacement amplitude X_0.

B. Complex Modulus

A second linear characterization approach is to characterize the complex damper stiffness K^* as the in-phase or storage stiffness K'

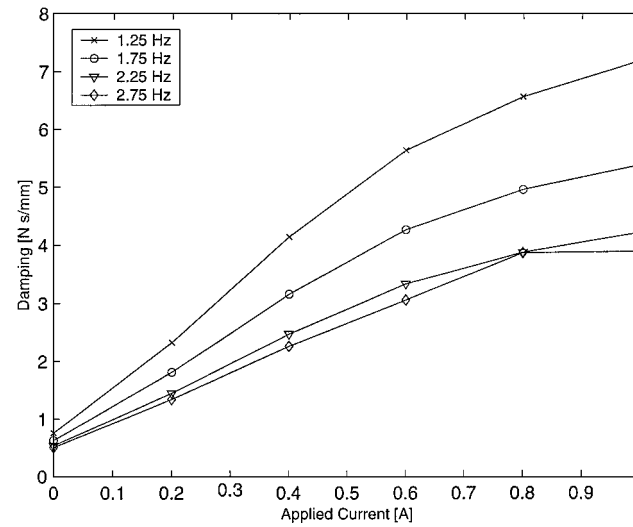

Fig. 3 Equivalent viscous damping is plotted vs applied current for several tested frequencies.

and quadrature or loss stiffness K'' so that

$$K^* = K' + jK'' = K'(1 + j\eta) \tag{4}$$

where η is the loss factor. This is a common approach in the characterization of elastomeric dampers.[2,22–24] To determine the damper force,

$$\begin{aligned} f(t) &= F_c \cos \Omega t + F_s \sin \Omega t \\ &= K'x(t) + (K''/\Omega)v(t) \end{aligned} \tag{5}$$

Here F_c and F_s are the cosine and sine Fourier coefficients of $f(t)$ at frequency Ω. We assume that the displacement is sinusoidal:

$$x(t) = X_c \cos \Omega t + X_s \sin\ \Omega t \tag{6}$$

where X_c and X_s are the cosine and sine Fourier coefficients of $x(t)$ at frequency Ω. Substituting $x(t)$ into the force equation and equating the sine and cosine terms yields the in-phase and quadrature stiffnesses as

$$K' = \frac{F_c X_c + F_s X_s}{X_c^2 + X_s^2}, \qquad K'' = \frac{F_c X_s - F_s X_c}{X_c^2 + X_s^2} \tag{7}$$

The storage stiffness K' is sometimes called the *effective* or *equivalent stiffness*. The loss stiffness K'' is approximately related to the equivalent viscous damping by

$$C_{\text{eq}} \approx K''/\Omega \tag{8}$$

The relation is approximate because the complex stiffness considers only the harmonic of the force at frequency Ω, whereas the equivalent damping considers all harmonics of the force.

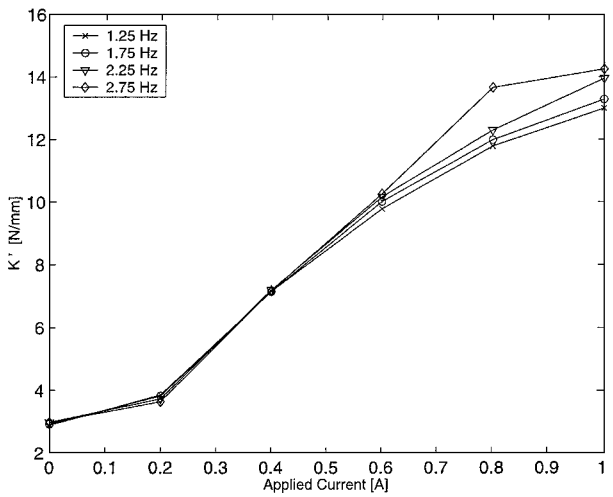

Fig. 4a Storage stiffness K' vs applied current.

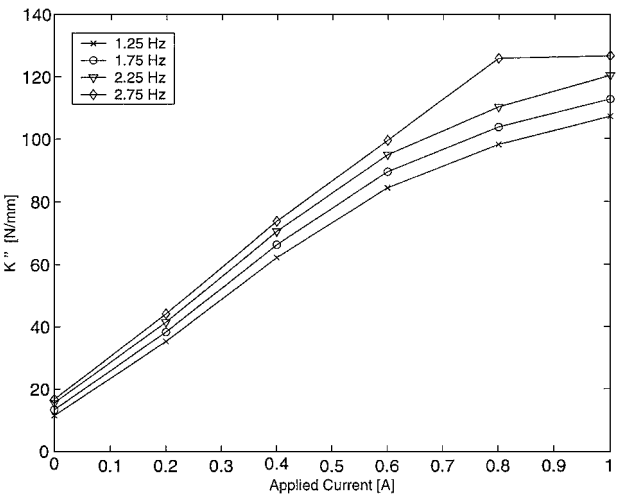

Fig. 4b Quadrature stiffness K'' vs applied current.

The estimated values for the equivalent stiffness and the loss stiffness for varying fields and shown in Figs. 4a and 4b. The damping and stiffness values increase as a quadratic function of the field.

VI. Nonlinear Damper Models

We discuss four perspectives with which to describe the behavior of the MR damper for oscillatory sinusoidal loading conditions: 1) nonlinear Bingham plastic model,[9,10] 2) nonlinear biviscous model,[11,12] 3) a nonlinear hysteretic biviscous model, and 4) nonlinear viscoelastic plastic model.[8,14,15] The first three models are piecewise continuous in velocity, and the fourth model is piecewise smooth in velocity.

A. Bingham Plastic Model

By adding a yield force to a linear damping model, the nonlinear Bingham plastic model results. This shear flow mechanism has been used to develop predictive models assuming both parallel plate geometry[25–27] or axisymmetric geometry.[20,21,28] Yield force F_y and postyield damping C_{po} are included in the model. A schematic of this model is shown in Fig. 5a. The equations describing this damper model are

$$f(t) = \begin{cases} C_{\text{po}} v + F_y & v > 0 \\ -F_y < f(t) < F_y & v = 0 \\ C_{\text{po}} v - F_y & v < 0 \end{cases} \tag{9}$$

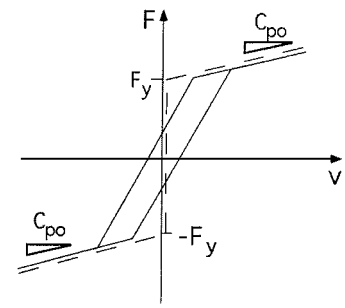

a) Nonlinear Bingham plastic

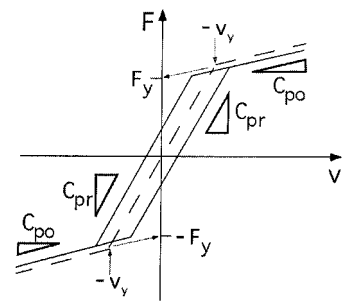

b) Nonlinear biviscous

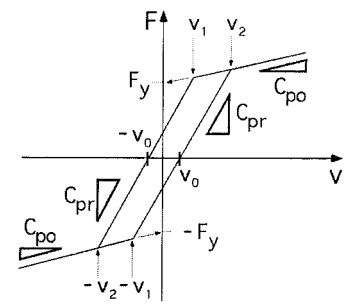

c) Nonlinear hysteretic biviscous

Fig. 5 Schematics of piecewise continuous nonlinear damper models. The idealized model force vs velocity behavior is represented by a – – –, whereas the —— is representative of actual damper behavior.

The nonlinear Bingham plastic model is often expressed as

$$f(t) = F_y \,\mathrm{sign}[v(t)] + C_{\mathrm{po}} v(t) \tag{10}$$

The model assumes that in the preyield condition the material is rigid and does not flow; hence, when $|f(t)| < F_y$ the shaft velocity $v = 0$. Once the force applied to the damper exceeds the yield force, then the fluid begins to flow, and the material is essentially a Newtonian fluid with a nonzero yield stress, as shown in Fig. 5a. In this damper model the yield force is obtained from the postyield force vs velocity asymptote intercept with the force axis, as shown in Fig. 5a.

B. Nonlinear Biviscous Model

Rather than assuming that the MR fluid is rigid in the preyield condition, we adopt the nonlinear biviscous model developed by Stanway et al.,[11] where it is assumed the MR fluid is plastic in both the preyield and the postyield conditions. However, the preyield damping C_{pr} should be assumed to be much greater than the postyield damping C_{po} or $C_{\mathrm{pr}} > C_{\mathrm{po}}$. In this damper model the yield force is still represented by the postyield force vs velocity asymptote intercept with the force axis, as shown in Fig. 5b. The advantage of a plastic preyield mechanism is that it accounts for the preyield damping portion of the typical viscoelastic preyield behavior of an ER or MR fluid. Versions of this model have been adopted to analyze leakage in ER dampers.[12,29] The equations describing this model are

$$f(t) = \begin{cases} C_{\mathrm{po}} v + F_y & v \geq v_y \\ C_{\mathrm{pr}} v & -v_y \geq v \leq v_y \\ C_{\mathrm{po}} v - F_y & v \leq -v_y \end{cases} \tag{11}$$

where the yield velocity is given by

$$v_y = F_y / (C_{\mathrm{pr}} - C_{\mathrm{po}}) \tag{12}$$

C. Nonlinear Hysteretic Biviscous Model

Based on damper behavior observed during testing, the force vs velocity behavior shows a distinct preyield hysteresis. A four-parameter nonlinear hysteretic biviscous model that has a clear physical motivation is introduced. The nonlinear hysteretic biviscous model is an extension of Stanway et al.'s nonlinear biviscous constitutive model[11] with an improved representation of the preyield hysteresis. The preyield hysteresis is modeled by adding a fourth parameter, that is, the zero force velocity intercept v_0 to the three prior parameters: the preyield viscous damping C_{pr}, the postyield viscous damping C_{po}, and the yield force F_y. The equations of the piecewise continuous nonlinear hysteretic biviscous model, schematized in Fig. 5c, are

$$f(t) = \begin{cases} C_{\mathrm{po}} v - F_y & v \leq -v_1 & \dot{v} > 0 \\ C_{\mathrm{pr}}(v - v_0) & -v_1 \leq v \leq v_2 & \dot{v} > 0 \\ C_{\mathrm{po}} v + F_y & v_2 \leq v & \dot{v} > 0 \\ C_{\mathrm{po}} v + F_y & v_1 \leq v & \dot{v} < 0 \\ C_{\mathrm{pr}}(v + v_0) & -v_2 \leq v \leq v_1 & \dot{v} < 0 \\ C_{\mathrm{po}} v - F_y & v \leq -v_2 & \dot{v} < 0 \end{cases} \tag{13}$$

where we have introduced the compressive yield velocity v_1 and the tensile yield velocity v_2, given by

$$v_1 = \frac{F_y - C_{\mathrm{pr}} v_0}{C_{\mathrm{pr}} - C_{\mathrm{po}}}, \qquad v_2 = \frac{F_y + C_{\mathrm{pr}} v_0}{C_{\mathrm{pr}} - C_{\mathrm{po}}} \tag{14}$$

The hysteresis cycle is separated into two groups of equations. The first group of three equations are for positive acceleration, whereas the second three are for negative acceleration.

D. Nonlinear Viscoelastic Plastic Model

As shown by the experimental force vs velocity hysteresis cycle data in Fig. 2b, there are two distinct rheological domains over which the dampers operate: the preyield and postyield regions. The preyield region exhibits a strong hysteresis, which is typical of a viscoelastic material. The postyield region is plastic with a nonzero yield force, as in the nonlinear Bingham plastic, biviscous, and hysteretic biviscous models. The yield force varies as a function of the applied current (magnetic field), as observed from Fig. 2. We now describe the structure of the nonlinear viscoelastic plastic model, a block diagram of which is depicted in Fig. 6.

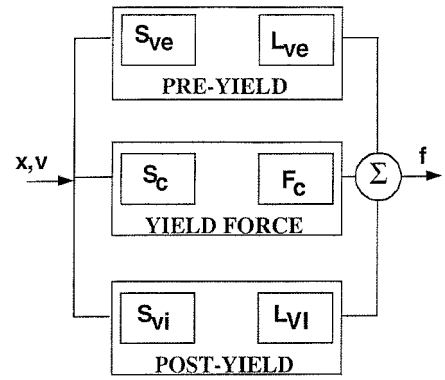

Fig. 6 Schematic of the nonlinear viscoelastic plastic model used to represent MR damper behavior.

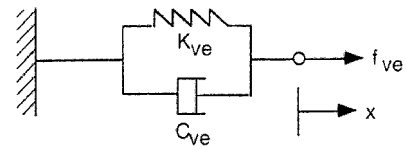

a) Viscoelastic mechanism L_{ve} in the preyield branch of the model

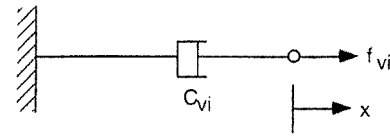

b) Viscous mechanism L_{vi} in the postyield branch of the model

Fig. 7 Mechanisms used in the viscoelastic plastic model.

1. *Preyield Mechanism*

The Kelvin chain element shown in Fig. 7a is used as the mechanical analog representing the viscoelastic behavior of the damper in the preyield region. The differential equation representing this mechanism in the time domain is

$$f_{\mathrm{ve}}(t) = K_{\mathrm{ve}} x(t) + C_{\mathrm{ve}} v(t) \tag{15}$$

Here f_{ve} is the viscoelastic component of the damper force. The nonlinear shape function S_{ve} is the preyield switching function, which along with an analogous postyield switching function S_{vi} effects the smooth transition from the preyield phase to the postyield phase. The function S_{ve} is dependent on the yield velocity v_y that is chosen during the estimation process. S_{ve} is given by

$$S_{\mathrm{ve}}(v) = \frac{1}{2}\left[1 - \tanh\left(\frac{|v| - v_y}{4\epsilon_y}\right)\right] \tag{16}$$

where $v(t)$ is the instantaneous velocity, and ϵ_y is a smoothening parameter. Thus, the force component caused by the preyield mechanism is given by

$$f_{\mathrm{pr}}(t) = S_{\mathrm{ve}}(v) f_{\mathrm{ve}}(t) \tag{17}$$

2. *Postyield Mechanism*

In postyield the damper clearly behaves as a viscous damper with a nonzero yield force. The postyield mechanical analog, denoted by L_{vi} in Fig. 6, is the viscous mechanism, which can be represented as a damper in Fig. 7b. Thus, the postyield force component is given by

$$f_{\mathrm{vi}} = C_{\mathrm{vi}} v(t) \tag{18}$$

S_{vi} is similar to the shape function S_{ve}, where S_{vi} acts as a switching function to turn on the postyield viscous mechanism when the damper crosses the yield point. It is given by

$$S_{\mathrm{vi}}(v) = \frac{1}{2}\left[1 + \tanh\left(\frac{|v| - v_y}{4\epsilon_y}\right)\right] \tag{19}$$

Thus, the force component caused by the postyield mechanism is given by

$$f_{po}(t) = S_{vi}(v) f_{vi}(t) \tag{20}$$

3. Yield Force

The yield force F_c is a function of the applied field and is the field-dependent parameter that provides the damper with its semi-active capabilities. The Coulomb force or yield force effect seen in the damper behavior at low velocity are described using the yield force parameter F_c and the shape function S_c as given by the equation

$$S_c(v) = \tanh(v/4\epsilon_c) \tag{21}$$

where $v(t)$ is the velocity amplitude and ϵ_c is the smoothening factor that ensures smooth transition from the negative to positive velocities and vice versa. The force component caused by the yield force is given by

$$f_c(t) = S_c(v) F_c \tag{22}$$

4. Mechanisms-Based Model

For a sinusoidal displacement input the force output of the nonlinear viscoelastic plastic model is written as

$$\begin{aligned} f(t) &= f_{pr}(t) + f_{po}(t) + f_c(t) \\ &= S_{ve}(v) f_{ve} + S_{vi}(v) f_{vi} + S_c(v) F_c \end{aligned} \tag{23}$$

or, the total force is a nonlinear combination of the forces from each of the linear mechanisms.

The viscoelastic-plastic model combines linear mechanisms using nonlinear shape functions. In addition, the preyield and postyield mechanical analogs, the shape functions, the yield force effect, and nonlinear combination of these component forces to obtain the total predicted force, are based on observed damper behavior.

VII. Parameter Identification

The parameters associated with the nonlinear damper models are identified by minimizing the mean squared error between the measured force and the force predicted by the model, subject to constraints that the parameters be positive. The model parameters are determined only from the identification data set. These procedures are briefly described next.

A. Nonlinear Hysteretic Biviscous Model

The parameters of the three piecewise continuous models C_{pr}, C_{po}, F_y, and v_0 were identified as a function of applied current (magnetic field) and frequency, using a constrained least-mean-squared (LMS) error minimization procedure using MATLAB® subroutines. Only a single optimization procedure is required to identify the parameters of the nonlinear hysteretic biviscous model, the parameters of which are used for all three nonlinear models: Bingham plastic,

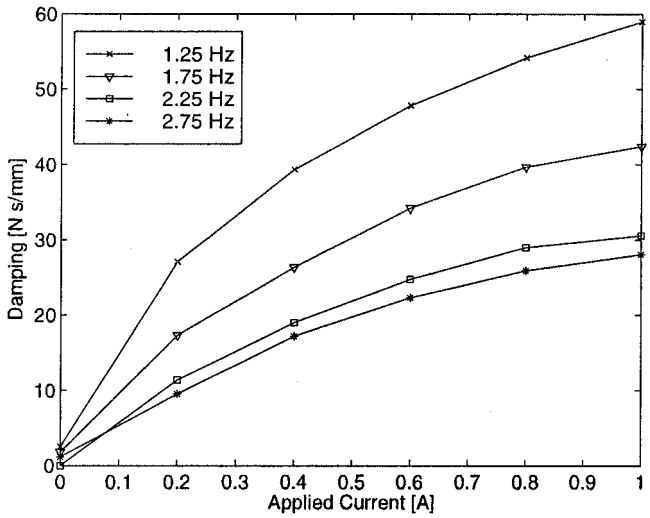

a) Preyield damping

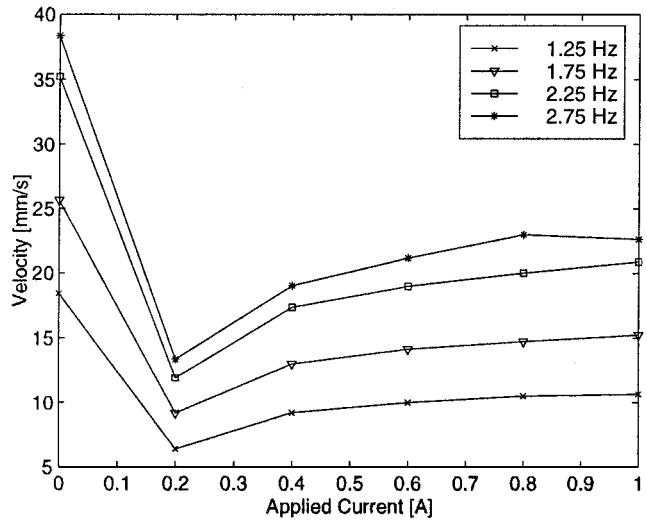

c) Zero force velocity intercept

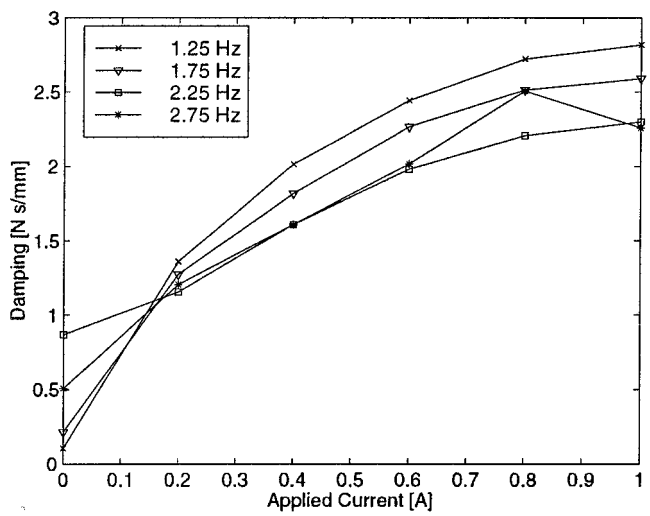

b) Postyield damping

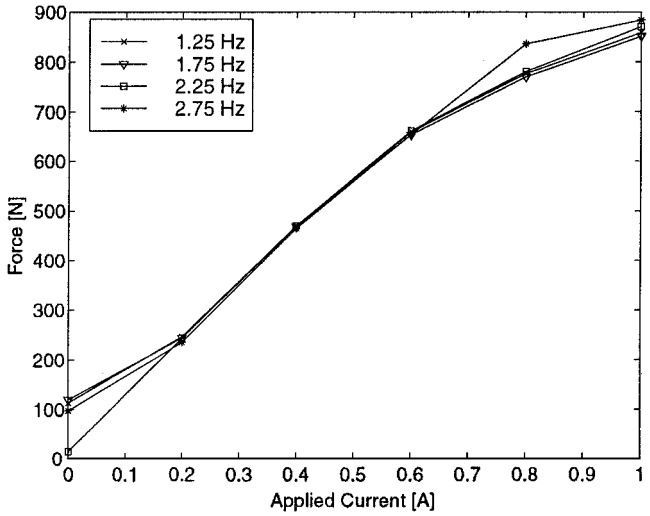

d) Yield force

Fig. 8 Four parameters of preyield damping C_{pr}, postyield damping C_{po}, zero force velocity intercept v_0, and yield force F_y are plotted vs applied current for the linear stroke MR damper.

biviscous, and hysteretic biviscous. A cost function J was defined as

$$J(C_{\mathrm{pr}}, v_0, C_{\mathrm{po}}, F_y) = \sum_{k=1}^{N} [f(t_k) - \hat{f}(t_k)]^2 \tag{24}$$

where $\hat{f}(t_k)$ is the force calculated using the equations of the nonlinear hysteretic biviscous model from Eq. (13), $f(t_k)$ is the measured force, and t_k is the time at which the kth sample was taken. The four parameters of C_{pr}, C_{po}, F_y, and v_0 are estimated so as to minimize the cost function J. The values of C_{pr}, C_{po}, F_y, and v_0 are all constrained to be greater than zero, and $C_{\mathrm{pr}} > C_{\mathrm{po}}$. The parameter optimization is performed on each test case of the identification data set. In Fig. 8 the four parameters of preyield damping C_{pr}, postyield damping C_{po}, zero force velocity intercept v_0, and yield force F_y are plotted vs applied current.

B. Nonlinear Viscoelastic Plastic Model

The parameters of the nonlinear viscoelastic plastic model C_{ve}, K_{ve}, C_{vi}, F_c, v_y, ϵ_y, and ϵ_c are functions of both applied field and frequency. In this case the cost function J was defined as

$$J(C_{\mathrm{ve}}, K_{\mathrm{ve}}, v_y, \epsilon_y, F_c, \epsilon_c, C_{\mathrm{vi}}) = \sum_{k=1}^{N} [f(t_k) - \hat{f}(t_k)]^2 \tag{25}$$

where $\hat{f}(t_k)$ is the force calculated using the equations of the nonlinear viscoelastic plastic model, $f(t_k)$ is the measured force, and t_k

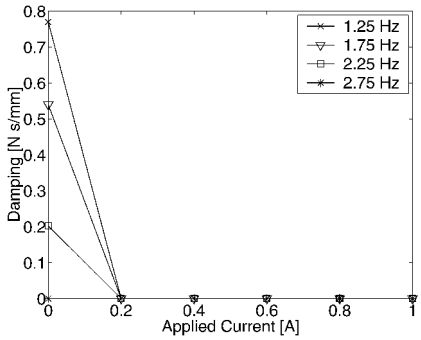

a) Preyield damping C_{ve}

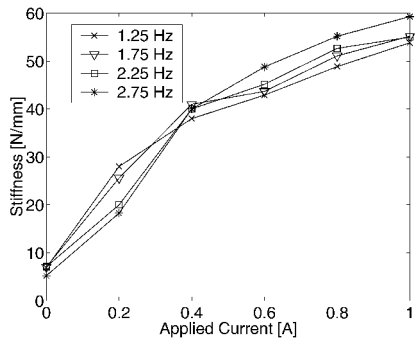

b) Preyield stiffness K_{ve}

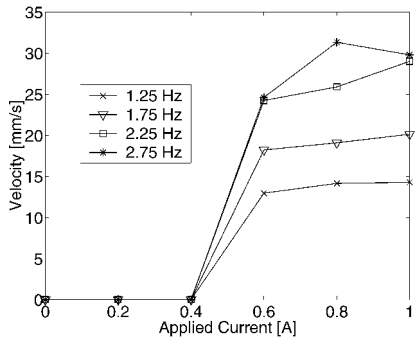

c) Yield velocity v_y

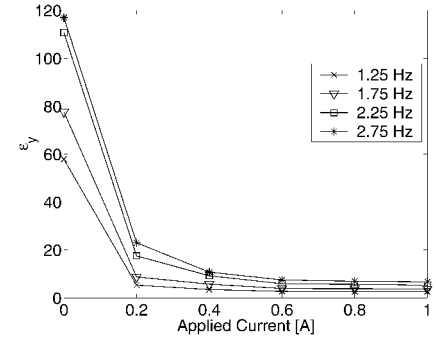

d) Yield parameter ϵ_y

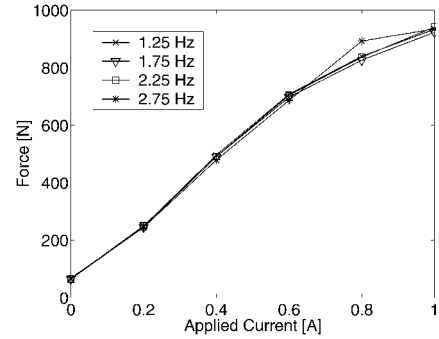

e) Yield force F_y

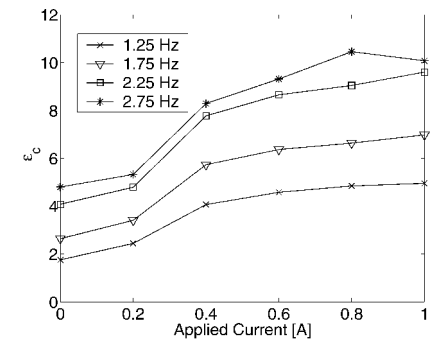

f) Yield force parameter ϵ_c

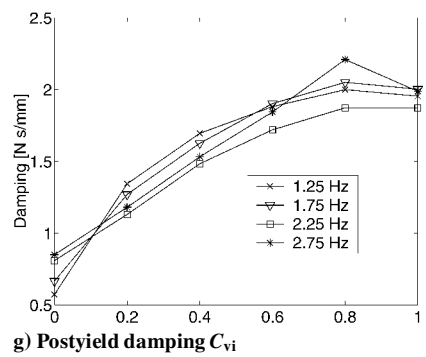

g) Postyield damping C_{vi}

Fig. 9 Parameters of the nonlinear viscoelastic plastic model are plotted vs applied current.

is the time at which the kth sample was taken. The seven parameters of the model are estimated so as to minimize the cost function J and are constrained to be greater than zero. The parameter optimization is performed for each tested condition of applied current and frequency.

An important problem is selecting the initial conditions for the optimizer. These initial conditions are based on the values calculated from the nonlinear hysteretic biviscous parameter optimization:

$$C_{\text{vi}} = C_{\text{po}}, \qquad F_c = F_y, \qquad v_y = v_0 \tag{26}$$

The initial conditions for the smoothening parameters ϵ_c and ϵ_y were typically chosen to be values between 0 and 10 depending on the test case. Initial conditions of the preyield mechanism parameters K_{ve} and C_{ve} were selected to be a small positive number and zero, respectively. In Fig. 9 the seven parameters of the viscoelastic plastic model plotted vs applied current.

VIII. Parameter Identification Results

The parameters obtained from the optimization procedure are used in their respective models to reconstruct hysteresis cycles. The force vs displacement and the force vs velocity cycles reconstructed from the parameters are then compared with the experimental data in the identification set.

A. Piecewise Continuous Models

The model parameters are used to reconstruct the force vs displacement and force vs velocity hysteresis cycles for each of the three piecewise continuous models. Figures 10–12 show the reconstructed hysteresis cycles using the optimized parameters for

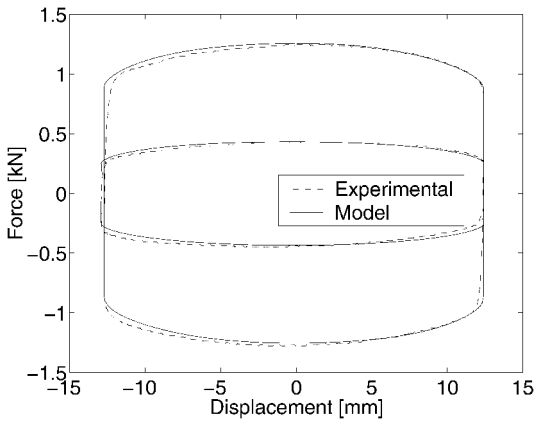

a) Bingham plastic force vs displacement

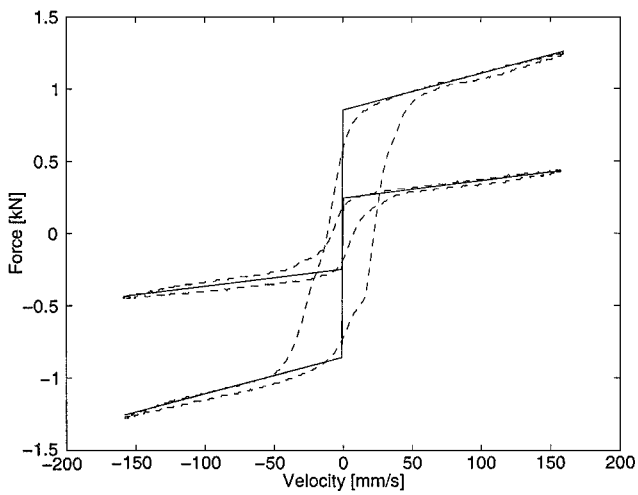

b) Bingham plastic force vs velocity

Fig. 10 Bingham plastic model reconstructions shown with experimental data. Test cases shown are I = 0.2, 1.0 A; Ω = 2.00 Hz.

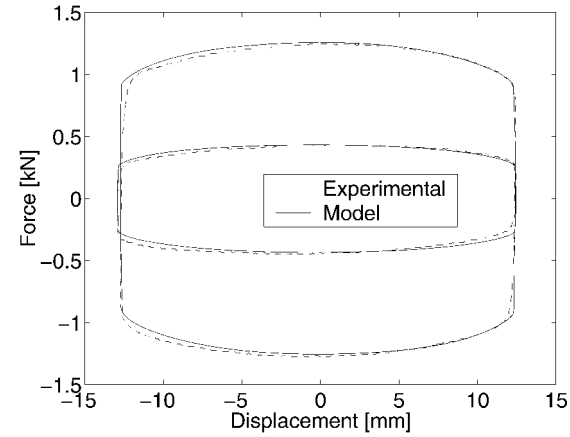

a) Biviscous force vs displacement

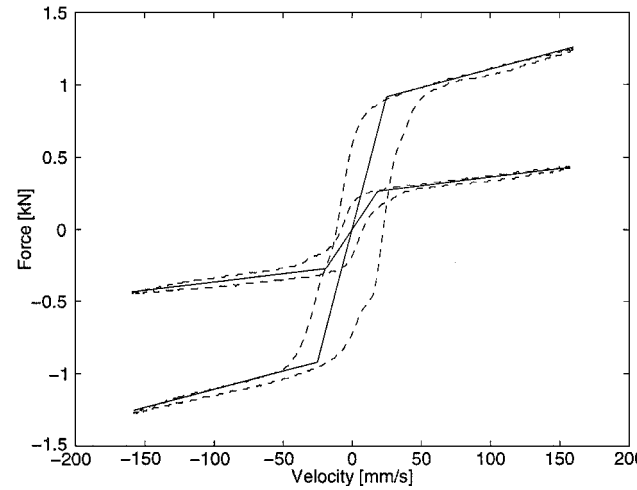

b) Biviscous force vs velocity

Fig. 11 Nonlinear biviscous model reconstructions shown with experimental data for test cases I = 0.2, 1.0 A; Ω = 2.00 Hz.

the nonlinear Bingham plastic, nonlinear biviscous, and the nonlinear hysteretic biviscous models. Applied currents of $I = 0.2$ and 1.0 A at a frequency of $\Omega = 2.0$ Hz are shown for each of the models.

For the nonlinear Bingham plastic model the comparison of modeled and experimental force vs displacement shown in Fig. 10a, the force vs velocity is shown in Fig. 10b. By adding a yield force to the postyield viscous damping, the Bingham plastic model accurately represents the postyield force vs velocity behavior. However, the rigid preyield characteristic is not representative of the measured preyield behavior.

For the nonlinear biviscous model the comparison of force vs displacement and force vs velocity is shown in Figs. 11a and 11b, respectively. The rigid preyield of the Bingham plastic model is replaced by a viscous preyield mechanism in order to have a more realistic preyield behavior. However, the preyield force vs velocity hysteresis is still not captured by this model.

For the nonlinear hysteretic biviscous model the force vs displacement and force vs velocity hysteresis cycles are shown in Figs. 12a and 12b. Of the piecewise continuous models the nonlinear hysteretic biviscous model most accurately represents the force vs velocity behavior, including the preyield hysteresis. The force vs displacement behavior is equally well represented by all of the piecewise continuous models.

B. Piecewise Smooth Model

The optimized parameter values are used to reconstruct the force vs displacement and force vs velocity hysteresis cycles for all of the tested conditions of the identification set. Shown in Figs. 13a and

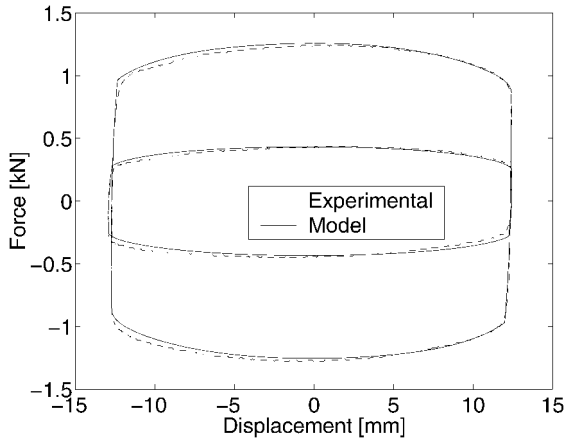

a) Hysteretic biviscous force vs displacement

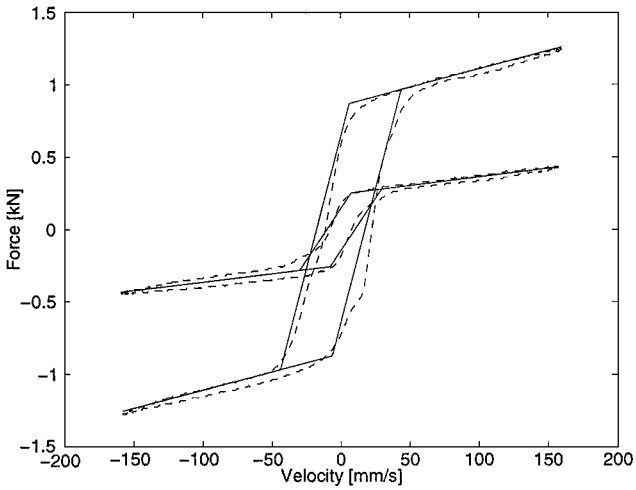

b) Hysteretic biviscous force vs velocity

Fig. 12 Hysteretic biviscous model reconstructions shown with experimental data for test cases $I = 0.2$, 1.0 A; $\Omega = 2.00$ Hz.

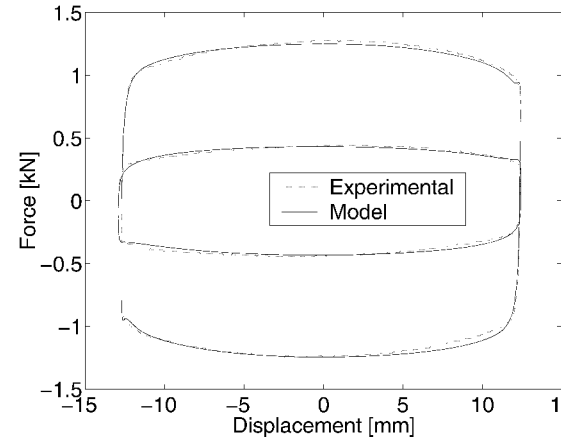

a) Viscoelastic plastic force vs displacement

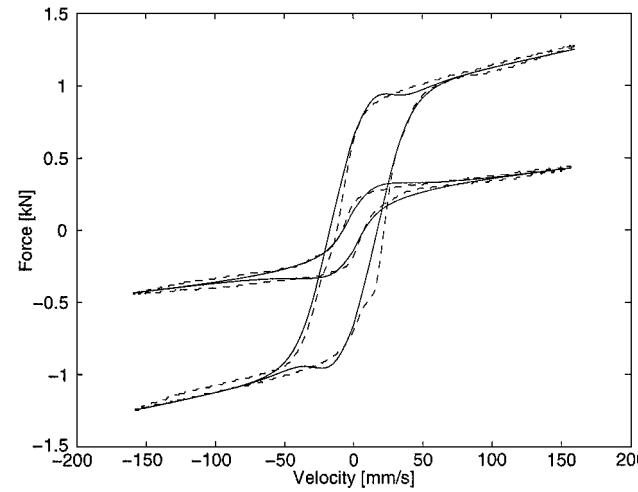

b) Viscoelastic plastic force vs velocity

Fig. 13 Viscoelastic plastic model reconstructions shown with experimental data for test cases $I = 0.2$, 1.0 A; $\Omega = 2.00$ Hz.

13b are the force vs displacement and force vs velocity hysteresis cycles for $\Omega = 2.0$ Hz for the applied current $I = 0.2$ and 1.0 A. This model very accurately reconstructs the force vs velocity behavior, including the preyield hysteresis. The force vs displacement data are also accurately reconstructed.

IX. Model Performance Assessment

To evaluate the performance of each of the four nonlinear models, the error between the experimental and the model values for the equivalent viscous damping and the force time history are calculated.

A. Equivalent Viscous Damping Error

Of critical importance is the modeling of damping or energy dissipation. Here we evaluate how well the nonlinear models identify the energy dissipation over one cycle because the cost function for the parameter optimization techniques was the LMS error in the prediction of the force time history and not the energy dissipation over a cycle. The force vs displacement hysteresis cycle behavior is represented accurately by the three nonlinear piecewise continuous models, but the nonlinear viscoelastic plastic model is a much improved model. The accuracy of the nonlinear models at matching the energy dissipation per cycle is fairly consistent, even though the force vs velocity hysteresis behavior varies significantly between the models. Essentially, the postyield behavior of the damper plays the largest role in describing the energy dissipation, where the velocity is greatest. All of the preyield behavior occurs at relatively lower velocity, making less of an impact on the damping performance.

To illustrate this, consider Figs. 14a and 14b, which show the error between the calculated damping from experimental data and the model during a single cycle of oscillation. Figure 14a shows the average equivalent viscous damping error for the Newtonian cases. The error for each model is obtained by taking the average error for the zero field, or Newtonian cases at all tested frequencies, and the standard deviation for each calculation is shown. As each model captures the hysteresis behavior more accurately, the equivalent viscous damping error is reduced. The overall performance for the Newtonian cases improves from 5.9% error for the Bingham plastic model to 0.1% for the viscoelastic plastic model.

Figure 14b shows the average equivalent viscous damping for the applied current cases, for which the damping error is much lower than for the Newtonian cases. This difference can be attributed to the asymmetric behavior seen in the damper when no field is applied. This effect is mainly caused by the nitrogen accumulator used to prevent cavitation. This asymmetry causes error in the identification of the model parameters, which are calculated using a symmetric model. As the applied field is increased, the hysteresis curves become symmetric because the effects of the accumulator diminish. At higher field strengths the model parameters can accurately be determined by the symmetric models, reducing the error. Figure 14b shows the average damping error for cases with applied field fall between 1.4% for the Bingham plastic model and 0.1% for the viscoelastic plastic model.

B. Force Error

As stated earlier, the postyield region behavior of the damper plays the largest role in the damper behavior. The ability of the

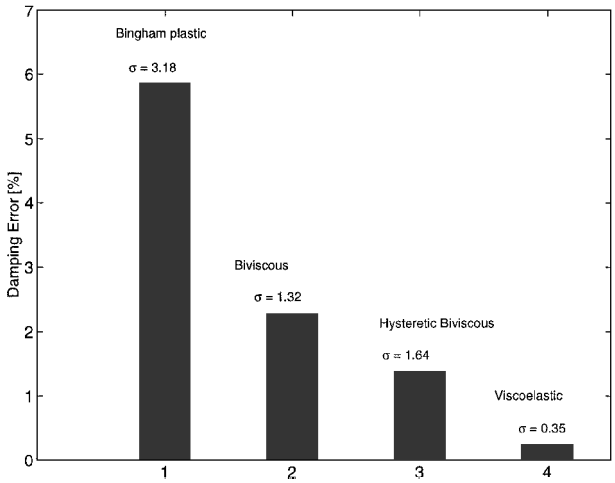

a) Zero field or Newtonian damping error

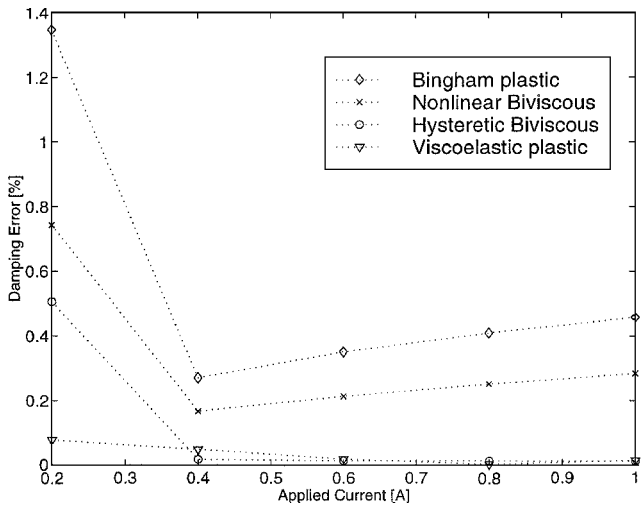

b) Damping error

Fig. 14 Average equivalent viscous damping errors for the identification data set.

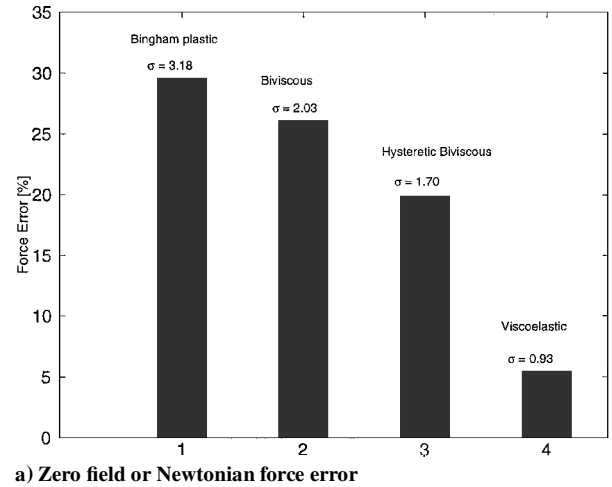

a) Zero field or Newtonian force error

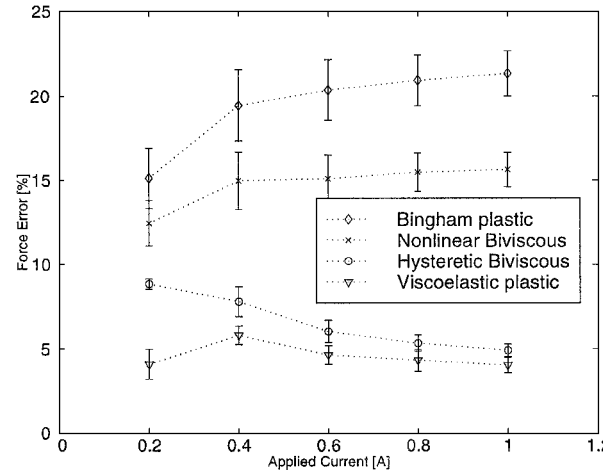

b) Force error

Fig. 15 Average force time history error for the identification data set.

nonlinear models to describe the force vs velocity hysteresis curves is extremely important in modeling the MR damper. To compare model performance in the identified force time history, the average error between the measured and identified force time histories is calculated. By calculating the force error for each model, we can get a quantitative measure of how well each model characterizes MR damper behavior. The force error was calculated using

$$\epsilon = \sqrt{\frac{1}{N}\sum_{k=1}^{N}[f(t_k) - \hat{f}(t_k)]^2} \Big/ f_{\max} \tag{27}$$

where $\hat{f}(t_k)$ is the force time history calculated using the equations for each of the models, $f(t_k)$ is the measured force, and t_k is the time at which the kth sample was taken. The rms value is then nondimensionalized by the maximum measured force. For each test case of the identification set the force error was calculated for all four models. These values were then used to calculate an average error for value of field tested.

Figure 15a shows the force error for the Newtonian cases from the identification data set. Again the error is the largest for the Bingham plastic model and decreases as the modeling of the preyield region improves. The error for the Bingham plastic model was 29.5% while the error for the viscoelastic plastic model was 5.5%. The biviscous and the hysteretic biviscous models fall within the range of error between the Bingham plastic and the viscoelastic plastic models.

Figure 15b compares the average force error for non-Newtonian cases for each of the four nonlinear models. Once again the effects of the preyield modeling are seen in the force error. The Bingham plastic model has an average error of 19.4%; with the addition of parameters and smoothing functions to create the viscoelastic plastic model, the force time history error is reduced to 4.5%. These results were generally expected; however, the performance of the hysteretic biviscous model was better than expected with 6.6% error. For higher field cases the nonlinear hysteretic biviscous model performed almost as well as the viscoelastic plastic model.

X. Computational Expense

Determining the model parameters through an optimization scheme is both time consuming and costly. When considering which model optimization scheme to use, the tradeoff between model performance and computational time should be considered.

The nonlinear hysteretic biviscous model has four model parameters that must be optimized for every test case. These four model parameters are essentially LMS line fits to the preyield and postyield regions of the force vs velocity data. This optimization is fairly simple, and the optimization of the four model parameters is very efficient. In fact the model parameters of the hysteretic biviscous model can be determined graphically with great accuracy.

The nonlinear viscoelastic plastic model is a piecewise smooth model that has seven parameters. Increasing the number of parameters increases the computational time required to minimize the cost function. Optimization time is also increased because the viscoelastic plastic model is a more complex curve fit than the LMS line fit, which the hysteretic biviscous model uses.

To compare the two models, the CPU running time and the number of flops for each optimization scheme were determined for three test cases representing a low, medium, and a high field strength test. The

applied current values were $I = 0.2$ A, 0.6 A, and 1.0 A; the frequency for each of these tests was $\Omega = 2.0$ Hz. Table 3 shows the results from the optimization cases for each model.

Typically the viscoelastic plastic model optimization is 16 times longer than the nonlinear hysteretic biviscous model optimization in terms of CPU processing time and uses three times as many more flops in order to minimize the cost function. The main difficulty that arises with this optimization scheme, other than actual running time, is choosing of initial conditions for each of the seven parameters.

Difficulties with the optimization are caused by incorrectly choosing initial values for each of the seven model parameters. Convergence for the parameters was unlikely to occur if even one of the initial values was chosen incorrectly. Because four of the model parameters are based on the four parameters of the hysteretic biviscous model, it is almost crucial that the nonlinear hysteretic biviscous optimization be run first to obtain values for those four parameters, which are in the correct range. As for the other three parameters, a trial and error method was used for these initial values. The sensitivity to initial conditions makes the nonlinear viscoelastic plastic model optimization scheme both more difficult and more time consuming to use. Quite often in this study test cases had to be run several times to obtain an acceptable fit with the experimental data.

Table 3 Computation effort comparison for the hysteretic biviscous and the viscoelastic models

Parameter	0.2 A	0.6 A	1.0 A
Hysteretic biviscous model optimization results			
Flops, M	4.6	4.5	5.8
CPU time, s	29	37	43
Viscoelastic plastic model optimization results			
Flops, M	12.9	13.3	16.6
CPU time, s	575	593	733

The results from the optimizations show that the viscoelastic plastic model gives slightly better results than the hysteretic biviscous in terms of modeling the damping and force, but a computational price is paid. The hysteretic biviscous model has an advantage with regard to optimization time because of its simplicity. Typically the performance of the hysteretic biviscous is fairly good with respect to the modeling of the hysteresis curves, making the hysteretic biviscous model better for some types of applications. When considering which model to use, performance as well as computational time and expense should be considered.

XI. Model Validation

The four nonlinear models require experimental data consisting of displacement, force, velocity, and acceleration in order to use the parameter optimization schemes. The prediction of hysteresis cycles from already identified model parameters is useful when experimental data are not available. To validate the model parameters over the operating range of the damper, a validation study was done. For this validation study the hysteretic biviscous and the viscoelastic plastic model parameters from the identification data set were used to determine offset model parameter values.

To determine the offset model parameters for the validation, a two-dimensional interpolation subroutine in MATLAB was used. Once

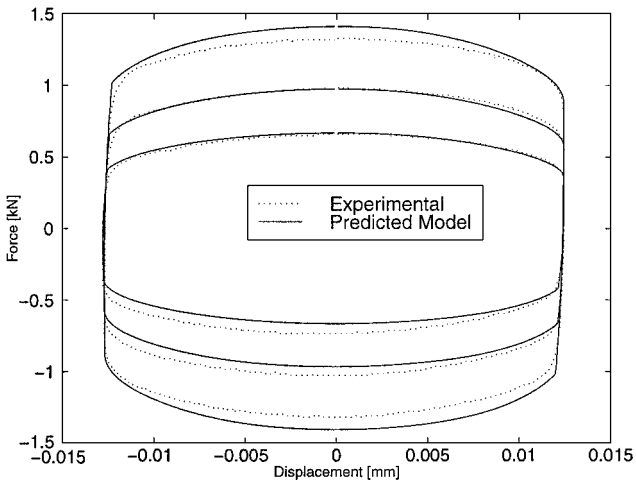

a) Hysteretic biviscous force vs displacement

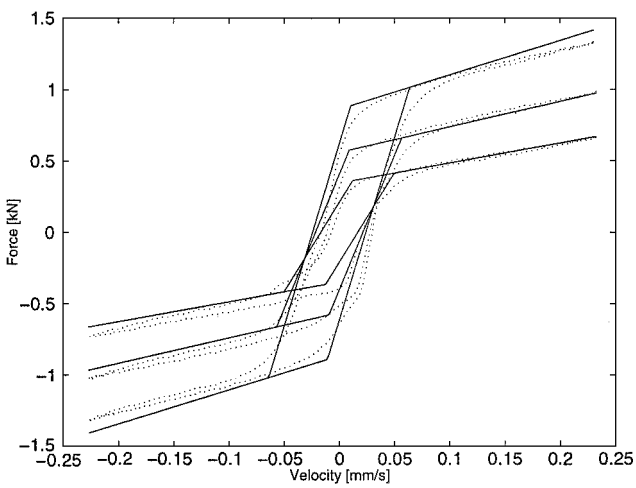

b) Hysteretic biviscous force vs velocity

Fig. 16 Predicted hysteresis cycles for the hysteretic biviscous model are compared to those from the validation data set. Test cases shown are I = 0.3, 0.5, and 0.9 A, all at 2.875 Hz.

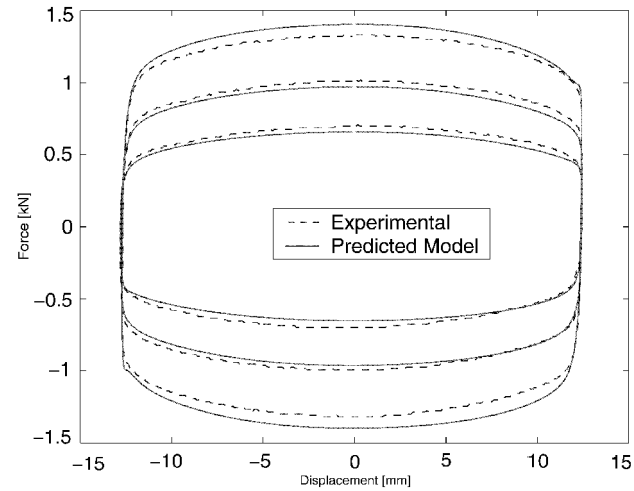

a) Viscoelastic plastic force vs displacement

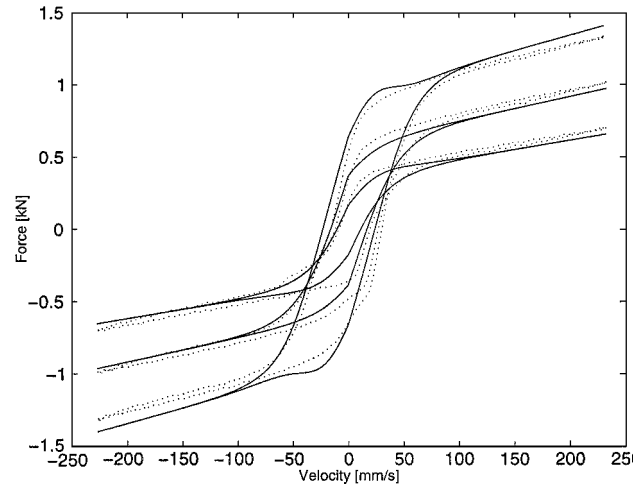

b) Viscoelastic plastic force vs velocity

Fig. 17 Predicted hysteresis cycles for the viscoelastic plastic model are compared to those from the validation data set. Test cases shown are I = 0.3, 0.5, and 0.9 A, all at 2.875 Hz.

the offset parameters were calculated, they were used to reconstruct force vs displacement and force vs velocity hysteresis cycles. The predicted hysteresis curves are compared with the experimental data from the validation data set. These data were collected at the same frequency and applied current as the predicted parameters.

Figures 16 and 17 show both the predicted and experimental hysteresis cycles for both the nonlinear hysteretic biviscous and the nonlinear viscoelastic plastic models. Each of the plots show applied current of 0.3, 0.5, and 0.9 A, at a frequency of $\Omega = 2.875$ Hz.

Figures 16a and 16b compare the measured force vs displacement and force vs velocity hysteresis cycle, with those predicted using the hysteretic biviscous model. Figures 17a and 17b do the same for the nonlinear viscoelastic plastic model. From these plots we can see that the correlation between the predicted and experimental hysteresis cycles is acceptable.

A. Model Prediction Error

To evaluate model performance, once again the equivalent viscous damping and the force time history errors are calculated. These errors will be used to compare the performance of the hysteretic biviscous and the viscoelastic plastic models in the validation study, which are compared with the results of the identification set.

B. Equivalent Viscous Damping Error

The equivalent viscous damping error for the prediction set is calculated using the same method that was used for the identification set. The Newtonian test cases were again separated from the applied field cases because the errors were higher as a result of the asymmetric behavior of the damper caused by the nitrogen accumulator.

First, examining the performance of each model in the prediction set in Figs. 18a and 18b shows the average Newtonian damping error for the nonlinear hysteretic biviscous and the viscoelastic plastic models. The zero field error for the viscoelastic plastic model is 29.1%; this is much higher than the error for the hysteretic biviscous model, which is 13.8%. Examining the non-Newtonian average damping errors, the 0.1 A case for both the hysteretic biviscous and the viscoelastic plastic has errors larger than the higher applied field cases. This is again caused by the asymmetric behavior of the damper at Newtonian and low field conditions. As the applied field increases, the average damping error decreases for both models, the average damping error for the nonlinear hysteretic biviscous model is 5.1%, and the average error for the nonlinear viscoelastic plastic model is 6.2%.

To compare the damping results from the identification set with those from the prediction set, consider Figs. 14 and 18. We can see that the equivalent viscous damping error is much higher in the prediction set than it is in the identification set for all field cases. The average Newtonian damping error of the prediction set is 13.8% for the hysteretic biviscous model; for the identification set this error is approximately 1.5%. For the applied field cases the average error for the equivalent viscous damping is 0.1% for the identification set; this error is on average 5.5% for the prediction data set.

Comparing the performance of the viscoelastic plastic model in the identification and prediction data sets, it is seen that the ability of the model to predict damping is not as good as the hysteretic biviscous model. The average damping error of the identification set was 0.1%, which is much lower than the average damping error for the validation set, which is 6.2%.

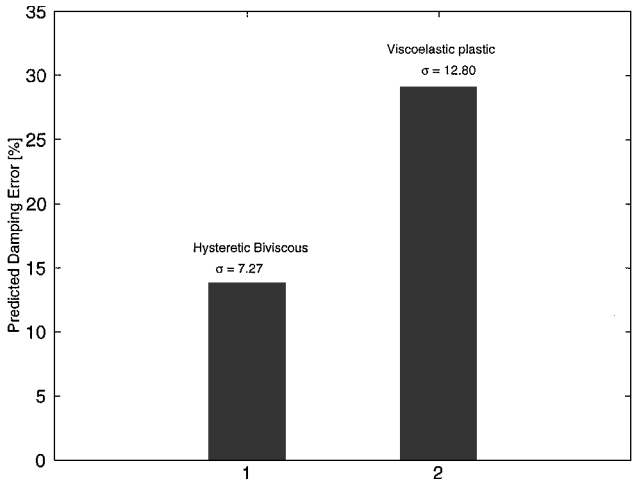

a) Newtonian prediction damping error

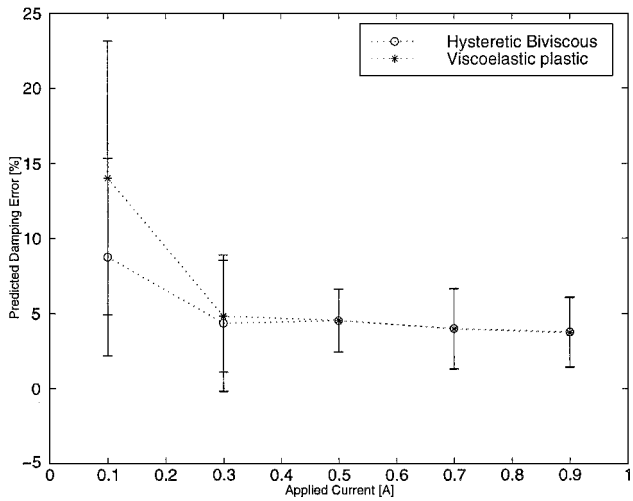

b) Prediction damping error

Fig. 18 Average damping error calculated from the predicted models and the experimental data.

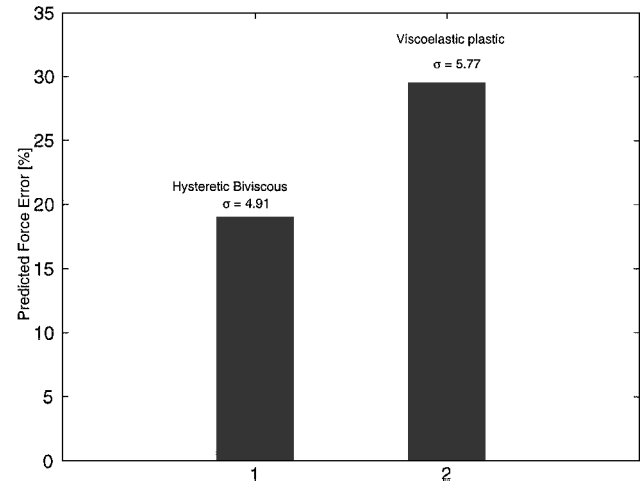

a) Newtonian prediction force error

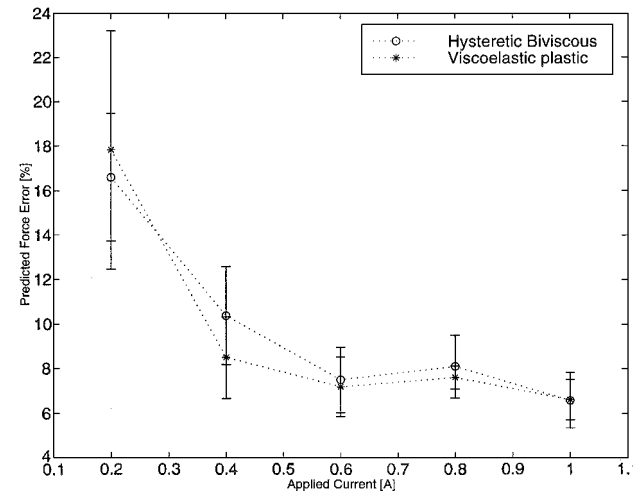

b) Prediction force error

Fig. 19 Average force time history error calculated from the predicted models and the experimental data.

C. Force Error

The force time history error between the predicted models and the measured force from the validation data set was calculated using Eq. (27). The results are shown in Figs. 19a and 19b.

The nonlinear hysteretic biviscous predicted model results were better than the viscoelastic plastic results for the Newtonian cases. The average Newtonian force error for the hysteretic biviscous model was approximately 19%, whereas the viscoelastic plastic Newtonian error was 29.5%. For the applied current cases the predictions were much better for both models. As the current increased the error decreased, and the models performed comparably. For the higher field strengths the average force error for both models is 9.5%. Comparing the force errors from the predictions with the force errors from the identification set, we see that the hysteretic biviscous model has about the same Newtonian force error in both studies. The viscoelastic plastic model percent error increased from 4.5% in the identification to 29.5% in the prediction. The two models perform comparably in both studies for applied field cases.

XII. Conclusions

An MR damper was characterized using equivalent viscous damping. This linear technique appropriately accounts for the energy dissipated over one oscillation cycle. This model describes the MR damper as an equivalent linear passive hydraulic damper via the equivalent viscous damping C_{eq}. C_{eq} was shown to be a function of both the applied magnetic field (current) and sinusoidal excitation. However, the equivalent viscous damping model does not accurately account for either the steady state force vs displacement or velocity hysteresis cycle behavior. Thus, the strong nonlinear behavior of the MR damper renders the linearized model nearly useless as a simulation model. However, C_{eq} is useful when comparing passive hydraulic or elastomeric dampers to MR dampers.

Four nonlinear models—the Bingham plastic, nonlinear biviscous, nonlinear hysteretic biviscous, and nonlinear viscoelastic plastic models—were proposed as the underlying model structure of a system identification procedure using experimental force vs displacement and force vs velocity hysteresis cycle data. These four models all describe the force vs displacement hysteresis cycles fairly well, but the nonlinear hysteretic biviscous and the nonlinear viscoelastic plastic models improve the reconstruction of the force vs velocity behavior. Improvements to the nonlinear Bingham plastic and the nonlinear biviscous model were made with additional model parameters and smoothing functions. A key conclusion of this study is that the preyield behavior has a small impact on the damping performance, but has a large impact in understanding the rheological behavior of the damper. For the four models the error in the damping performance was less than 6% for Newtonian cases and less than 1.4% for applied field cases.

The nonlinear hysteretic biviscous model has an advantage over the nonlinear viscoelastic plastic model in that the parameters can be estimated graphically from experimental data using linear or LMS fit procedures. Errors between the measured and model equivalent viscous damping were below 1%, whereas errors between the experimental force and the model force were typically around 6.6%. Because of the nonlinear hysteretic biviscous models ability to characterize damping, this model is the most appropriate as a simulation model for steady-state oscillations.

The nonlinear viscoelastic plastic (NVEP) model[8,14,15] is a piecewise smooth version of the nonlinear hysteretic biviscous model, which differs in that it is piecewise smooth in velocity. Force vs displacement and velocity hysteresis cycles were accurately reconstructed using this model. The energy dissipation error was far better for the NVEP model than for any of the other nonlinear models considered with a typical error less than 0.1%. The nonlinear viscoelastic plastic model also outperformed the nonlinear piecewise continuous models when reconstructing the force vs velocity hysteresis cycles. The average force time history error for the identification data set was 4.5%; this was on average 3% better than the nonlinear hysteretic biviscous model for higher field cases. The difference between the errors is even greater for low field cases.

A prediction study was also done using the nonlinear hysteretic biviscous and the nonlinear viscoelastic plastic models. These two models were chosen because of their superior performance over the Bingham plastic and nonlinear biviscous models in reconstructing the force vs velocity hysteresis cycles. Predicted model parameters were interpolated using the parameters identified using the identification data set. The values for the parameters were interpolated for intermediate current and frequency values. Hysteresis cycles were reconstructed from predicted parameters and compared with experimental data collected from the MR damper in the validation data set. Results of the prediction study show that the models performed comparably. Although prediction errors of equivalent viscous damping and force were higher than those errors in the identification set, the errors are still typically less than 10% for higher field cases.

Acknowledgments

Research was supported by the U.S. Army Research Office Young Investigator Program, Contract 38856-EG-YIP (Gary Anderson, Technical Monitor). Laboratory equipment was provided under a grant by the FY96 Defense University Research Instrumentation Program, Contract DAAH-0496-10301 (Gary Anderson, Technical Monitor). R. A. Snyder was supported in part under fellowships from the Vertical Flight Foundation. We also thank Mark Jolly, Lord Corporation, for his technical assistance.

References

[1]Carlson, J. D., Catanzarite, D. M., and St. Clair, K. A., "Commercial Magnetorheological Fluid Devices," *Proceedings of the International Conference on Electro-Rheological, Magneto-Rheological Suspensions and Associated Technology*, World Scientific Press, Rivers Edge, NJ, 1995, pp. 20–28.

[2]Kamath, G. M., Wereley, N. M., and Jolly, M. R., "Analysis and Testing of a Model-Scale Magnetorheological Fluid Helicopter Lag Mode Damper," *Journal of the American Helicopter Society*, Vol. 44, No. 3, 1999, pp. 234–248.

[3]Ervin, R. D., Lou, Z., Filisko, F. E., and Winkler, C. B., "Electrorheology for Smart Landing Gear," NASA CR-2000883 (N96-25313), April 1996.

[4]Lou, Z., Ervin, R. D., Filisko, F. E., and Winkler, C. B., "An Electrorheologically Controlled Semi-Active Landing Gear," Society of Automotive Engineers, Paper 93-1403, 1993.

[5]Leitmann, G., "Semiactive Control for Vibration Attenuation," *Journal of Intelligent Material Systems and Structures*, Vol. 5, No. 6, 1994, pp. 841–846.

[6]Leitmann, G., and Reithmeier, E., "A Control Scheme Based on ER-Materials for Vibration Attenuation of Dynamical Systems," *Applied Mathematics and Computation*, Vol. 70, 1995, pp. 247–259.

[7]Kunz, D. L., "Influence of Elastomeric Damper Modeling on the Dynamic Response of Helicopter Rotors," *AIAA Journal*, Vol. 35, No. 2, 1997, pp. 349–354.

[8]Kamath, G. M., and Wereley, N. M., "A Nonlinear Viscoelastic-Plastic Model for Electrorheological Fluids," *Smart Materials and Structures*, Vol. 6, No. 3, 1997, pp. 351–358.

[9]Prager, W., *Introduction to Mechanics of Continua*, Ginn and Co., New York, 1961, pp. 114–129.

[10]Phillips, R. W., "Engineering Applications of Fluids with a Variable Yield Stress," Ph.D. Dissertation, Mechanical Engineering, Univ. of California, Berkeley, CA, 1969.

[11]Stanway, R., Sproston, J. L., and El-Wahed, A. K. "Application of Electrorheological Fluids in Vibration Control: A Survey," *Smart Materials and Structures*, Vol. 5, No. 4, 1996, pp. 464–482.

[12]Wereley, N. M., and Lindler, J., E., "Biviscous Damping Behavior in Electrorheological Dampers," *ASME International Mechanical Engineering Congress and Exhibition: Adaptive Structures and Materials Symposium*, AD-Vol. 59/MD-Vol. 87, American Society of Mechanical Engineers, New York, 1999, pp. 67–75.

[13]Wereley, N. M., Pang, Li., and Kamath, K. M., "Idealized Hysteresis Modeling of Electrorheological and Magnetorheological Dampers," *Journal of Intelligent Material Systems and Structures*, Vol. 9, No. 8, 1998, pp. 642–649.

[14]Kamath, G. M., and Wereley, N. M., "Modeling the Damping Mechanism in Electrorheological Fluid Based Dampers," *M3DIII: Mechanics and Mechanisms of Material Damping*, edited by V. K. Kinra and A. Wolfenden, American Society for Testing and Materials, West Conshohocken, PA, 1997, pp. 331–348.

[15]Kamath, G. M., and Wereley, N. M., "Nonlinear Viscoelastic-Plastic Mechanisms-Based Model of an Electrorheological Damper," *Journal of Guidance, Control, and Dynamics*, Vol. 20, No. 6, 1997, pp. 1225–1332.

[16]Dyke, S. J., Spencer, B. F., Jr., Sain, M. K., and Carlson, J. D., "Modeling and Control of Magnetorheological Dampers for Seismic Response Reduction," *Smart Materials and Structures*, Vol. 5, No. 5, 1996, pp. 565–575.

[17]Spencer, B. F., Dyke, S. J., Sain, M. K., and Carlson, J. D., "Phenomenological Model of a Magnetorheological Damper," *Journal of Engineering Mechanics*, Vol. 123, No. 3, 1997, pp. 230–238.

[18]Weiss, K. D., Carlson, J. D., and Nixon, D. A., "Viscoelastic Properties of Magneto- and Electro-Rheological Fluids," *Journal of Intelligent Material Systems and Structures*, Vol. 5, No. 6, 1994, pp. 772–775.

[19]Bendat, J. S., and Piersol, A. G., *Random Data: Analysis and Measurement Procedures,* Wiley, New York, 1986, pp. 368–377.

[20]Kamath, G. M., Hurt, M. K., and Wereley, N. M., "Analysis and Testing of Bingham Plastic Behavior in Semi-Active Electrorheological Fluid Dampers," *Smart Materials and Structures*, Vol. 5, No. 5, 1996, pp. 576–590.

[21]Gavin, H. P., Hanson, R. D., and Filisko, F. E., "Electrorheological Dampers, Part I: Analysis and Design," *Journal of Applied Mechanics*, Vol. 63, No. 3, 1996, pp. 669–675.

[22]Felker, F. F., Lau, B. H., McLaughlin, S., and Johnson, W., "Nonlinear Behavior of an Elastomeric Lag Damper Undergoing Dual-Frequency Motion and its Effect on Rotor Dynamics," *Journal of the American Helicopter Society*, Vol. 32, No. 4, 1987, pp. 45–53.

[23]McGuire, D. P., "Fluidlastic Dampers and Isolators for Vibration Control in Helicopters," *50th Annual Forum of the American Helicopter Society*, American Helicopter Society, Alexandria, VA, 1994, pp. 295–304.

[24]Panda, B., and Mychalowycz, E., "Aeroelastic Stability Wind Tunnel Testing with Analytical Correlation of the Comanche Bearingless Main Rotor," *Journal of the American Helicopter Society*, Vol. 42, No. 3, 1997, pp. 207–217.

[25]Wereley, N. M., and Pang, Li, "Nondimensional Analysis of Semi-Active Electrorheological and Magnetorheological Dampers Using Approximate Parallel Plate Models," *Smart Materials and Structures*, Vol. 7, No. 5, 1998, pp. 732–743.

[26]Makris, N., Burton, S. A., Hill, D., and Jordan, M., "Analysis and Design of ER Damper for Seismic Protection of Structures," *Journal of Engineering Mechanics*, Vol. 122, No. 10, 1996, pp. 1003–1011.

[27]Lou, Z., Ervin, R. D., and Filisko, F. E., "A Preliminary Parametric Study of Electrorheological Dampers," *Electro-Rheological Flows*, FED-Vol. 164, American Society of Mechanical Engineers, New York, 1993, pp. 143–156.

[28]Gavin, H. P., Hanson, R. D., and Filisko, F. E., "Electrorheological Dampers, Part II: Testing and Modeling," *Journal of Applied Mechanics*, Vol. 63, No. 3, 1996, pp. 676–682.

[29]Lindler, J., and Wereley, N. M., "Parametric Analysis and Testing of an Electrorheological Fluid Damper," *Smart Structures and Materials 1999: Smart Structures and Integrated Systems*, edited by N. M. Wereley, Vol. 3668, *Proceedings of SPIE*, Society of Photo-Optical Instrumentation Engineers, Bellingham, WA, 1999, pp. 474–486.

A. Chattopadhyay
Associate Editor